Cover Page

Title: Cationic π-Stacking Columns of Coronene Molecules with Fully-Charged and Charge-Disproportionated States

Authors: Yukihiro Yoshida,* Kazuhide Isomura, Mitsuhiko Maesato, Takashi Koretsune, Yoshiaki Nakano, Hideki Yamochi, Hideo Kishida, and Gunzi Saito

Affiliations: Faculty of Agriculture, Meijo University, Tempaku-ku, Nagoya 468-8502, Japan, Department of Applied Physics, Nagoya University, Chikusa-ku, Nagoya 464-8603, Japan, Division of Chemistry, Graduate School of Science, Kyoto University, Sakyo-ku, Kyoto 606-8502, Japan, Center for Emergent Matter Science, RIKEN, Wako 351-0198, Japan, JST, PRESTO, Saitama 332-0012, Japan, Research Center for Low Temperature and Materials Sciences, Kyoto University, Sakyo-ku, Kyoto 606-8501, Japan, Toyota Physical and Chemical Research Institute, Nagakute 480-1192, Japan

Abstract: Electrochemical oxidation of a polycyclic aromatic hydrocarbon, coronene, with D_{6h} symmetry in the presence of tetrahedral $GaCl_4^-$ anions gave two cation salts, (coronene)($GaCl_4$) (**1**) and (coronene)$_5$($GaCl_4$)$_2$ (**2**), with unprecedented charge arrangements. Salt **1** involves π-stacking columns in a zig-zag manner, which are composed of crystallographically equivalent coronene monocations. First-principle calculations revealed that the dimerization of coronene cations gives rise to a band gap opening at the Fermi level, and thus, semiconducting behavior. On the other hand, in salt **2**, two crystallographically independent coronene molecules (**A** and **B**) form π-stacking columns with an **AABB** repeating unit, which are flanked by another coronene molecule (**C**). The crystallographic features, such as interplanar distances and in-plane molecular distortions arising from the Jahn-Teller effect, as well as the first-principle calculations, strongly suggested the emergence of charge disproportionation within the π-columns. As in the case of **1**, the

calculated band structure exhibits a band gap opening at the Fermi level, which corresponds to the observed semiconducting behavior.

Corresponding Author: Yukihiro Yoshida (Meijo University, Tel: +81-52-838-2552, Fax: +81-52-833-7200, E-mail: yyoshida@meijo-u.ac.jp)

Cationic π-Stacking Columns of Coronene Molecules with Fully-Charged and Charge-Disproportionated States

Yukihiro Yoshida,[*,†] *Kazuhide Isomura,*[‡] *Mitsuhiko Maesato,*[§] *Takashi Koretsune,*[#,¶] *Yoshiaki Nakano,*[§,⊥] *Hideki Yamochi,*[§,⊥] *Hideo Kishida,*[‡] *and Gunzi Saito*[†,||]

[†] Faculty of Agriculture, Meijo University, Tempaku-ku, Nagoya 468-8502, Japan

[‡] Department of Applied Physics, Nagoya University, Chikusa-ku, Nagoya 464-8603, Japan

[§] Division of Chemistry, Graduate School of Science, Kyoto University, Sakyo-ku, Kyoto 606-8502, Japan

[#] Center for Emergent Matter Science, RIKEN, Wako 351-0198, Japan

[¶] JST, PRESTO, Saitama 332-0012, Japan

[⊥] Research Center for Low Temperature and Materials Sciences, Kyoto University, Sakyo-ku, Kyoto 606-8501, Japan

[||] Toyota Physical and Chemical Research Institute, Nagakute 480-1192, Japan

Abstract: Electrochemical oxidation of a polycyclic aromatic hydrocarbon, coronene, with D_{6h} symmetry in the presence of tetrahedral $GaCl_4^-$ anions gave two cation salts, (coronene)($GaCl_4$) (**1**) and (coronene)$_5$($GaCl_4$)$_2$ (**2**), with unprecedented charge arrangements. Salt **1** involves π-stacking columns in a zig-zag manner, which are composed of crystallographically equivalent coronene monocations. First-principle calculations revealed

that the dimerization of coronene cations gives rise to a band gap opening at the Fermi level, and thus, semiconducting behavior. On the other hand, in salt **2**, two crystallographically independent coronene molecules (**A** and **B**) form π-stacking columns with an **AABB** repeating unit, which are flanked by another coronene molecule (**C**). The crystallographic features, such as interplanar distances and in-plane molecular distortions arising from the Jahn-Teller effect, as well as the first-principle calculations, strongly suggested the emergence of charge disproportionation within the π-columns. As in the case of **1**, the calculated band structure exhibits a band gap opening at the Fermi level, which corresponds to the observed semiconducting behavior.

Introduction

Self-assemblies, mainly through π-π interactions, of polycyclic aromatic hydrocarbons (PAHs), which form the backbone of organic electronics such as field-effect transistors, electroluminescence, and solar cell devices, have been attracted increasing interest in the materials science field for more than half a century.[1–3] In particular, the face-to-face π-stacking of radical species provides magnetic-exchange and electron-transfer pathways in the assemblies, which are essential for the developments of electronic functional materials. As a candidate for such a PAH, coronene, which is the smallest fragment of graphene with a central ring shared with six adjacent rings, is in a promising class of molecules that display metallic and superconducting behavior because of doubly degenerate frontier orbitals stemming from D_{6h} molecular symmetry.[4–6] It is worth noting that coronene has obvious chemical advantages over its two representative homologues, benzene and hexa-*peri*-hexabenzocoronene (Fig. 1); namely, they are fraught with drawbacks of high vapor pressure and low redox activity (*i.e.*, difficulty in obtaining stable charge transfer (CT) solids) for the former[7,8] and extremely low vapor pressure and solubility in common organic

solvents (*i.e.*, difficulty in purification and complex preparation) for the latter.[9–11] We recently obtained the first π-stacking columns composed of cationic coronene molecules by combining with octahedral M_6O_{19} cluster dianions (M = Mo^{VI}, W^{VI}),[12] as well as a series of alternating π-columns composed of coronene (D) and electron acceptor molecules (A) with DA- or DDA-type arrangement patterns.[6,13–15] However, the formation of dicationic coronene triads results in a band-insulating ground state. A wide variety of charge states within the coronene-based π-columns will inevitably enable elucidation of the relationship between charge arrangement and electronic states, which is necessary for determining their potential as electronic model materials. In addition, an increase in the number of such materials provides further clues for selecting counter components to obtain desired properties through crystal-chemical control.

********** Figure 1 **********

In this study, we obtained two kinds of unprecedented coronene cation salts by electrooxidation in the presence of tetrahedral $GaCl_4^-$ monoanions, bearing in mind that the shape (size and symmetry) and charge state of counter anions have a great influence on structural and electronic properties of the cation radical salts.[16,17] Whereas the 1:1 salt, (coronene)($GaCl_4$) (**1**), involves π-stacking columns composed of fully charged coronene molecules, the 5:2 salt, (coronene)$_5$($GaCl_4$)$_2$ (**2**), involves charge-disproportionated π-stacking columns flanked by another neutral coronene molecule. The crystallographic features, as well as the charge and electronic properties of the salts, were investigated using both experimental (single-crystal X-ray diffraction, Raman, and resistivity measurements) and theoretical methods.

Results and Discussion

Synthesis. Black rod-shaped crystals of **1** and **2** (Fig. S1 in the Supporting Information) were obtained by galvanostatic electrooxidation of coronene in the presence of $GaCl_4^-$ anions in dichloromethane/methanol mixed solution. Although these salts are indistinguishable from each other by their appearance, they can be more selectively obtained by changing the amounts of starting reagents (see Experimental section). The effects of reaction conditions such as current (1–5 μA), temperature (15–30 °C), and time (1–4 weeks) are not large enough to modify the obtained products. Both salts are rather unstable under aerobic conditions, and especially, salt **1** is made into an amorphous form upon exposure to air at room temperature for a few weeks. Notably, their durability in air is dramatically improved by storage at refrigerated temperatures. Crystallographic studies revealed that both salts undergo no structural phase transitions down to 100 K.

(coronene)($GaCl_4$) (1). Salt **1** crystallizes in a triclinic lattice with space group $P\bar{1}$,[18] and each coronene and $GaCl_4^-$ is crystallographically independent. As shown in Fig. 2, coronene molecules assemble in a zig-zag stacking manner along the *a* axis. Each coronene molecule is connected with two neighboring $GaCl_4^-$ anions through C–H···Cl hydrogen bonds (H1···Cl2: 2.87 Å, H10···Cl1: 2.87 Å vs. sum of van der Waals radii: 2.95 Å[19]), which result in the formation of a coronene dimer on an inversion center. Each coronene dimer has a ring-over-atom overlap motif with an interplanar distance of 3.28 Å, whereas ring-over-bond overlap is observed between the neighboring dimers with an interplanar distance of 3.27 Å (Fig. 2a). These distances are similar to those in cation salts, $(coronene)_3M_6O_{19}$, with π-columnar structures (3.16 Å for ring-over-atom and 3.19–3.21 Å for ring-over-bond)[12] and a dicationic coronene dimer, $(coronene)_2^{2+}$, as optimized by theoretical calculations (3.2 Å).[20] However, the distances are significantly shorter than those in natural graphite (3.35 Å; ring-over-atom),[21] a pristine coronene solid with a herringbone structure (3.43 Å;

ring-over-bond),[22] a neutral solid, (coronene)$_3$TCNQ (TCNQ: 7,7,8,8-tetracyano-*p*-quinodimethane), composed of alternating π-columns with a [coronene···coronene···TCNQ] repeating unit (3.43 Å; ring-over-atom),[13] and a neutral coronene dimer optimized by theoretical calculations (3.34–3.51 Å; ring-over-atom),[23–27] possibly because of charge resonance stabilization. The deformation of coronene molecules in **1** will be described later in detail.

********** Figure 2 **********

To assess the intermolecular interactions in **1**, band structure calculations were performed using the first principles method within density functional theory (DFT) based on the crystallographic data obtained at 100 K. It is apparent that the energy dispersions of the four highest branches in Fig. 3a are quite large along the stacking direction (//*a* axis) relative to those along the inter-columnar directions because of significant face-to-face π-π interactions. The first and fourth highest branches mainly derive from the b_{3u} orbital, whereas the corresponding second and third branches mainly derive from the a_u orbital. Within the column, the intermolecular transfer integrals between b_{3u} orbitals are –276 meV within a dimer and 135 meV between dimers, whereas those between a_u orbitals are estimated to be –120 meV within a dimer and 59 meV between dimers (Table S1). The b_{3u}-derived branches are apparently more dispersive than the a_u-derived ones, which is possibly a consequence of the higher transfer integrals. The width of the four bands was estimated to be 246, 80, 163, and 235 meV in higher order of energy level. The marked alternation in the intermolecular transfer integral between each of the orbitals closely corresponds to a significant energy difference between each of the branches derived from the b_{3u} or a_u orbital. The b_{3u}-derived bands are only 60 meV higher in energy than the a_u-derived bands, implying the presence of a

highly degenerate HOMO, even though the crystal field normally results in splitting of the doubly degenerate e_{2u} HOMO in D_{6h} symmetry into two non-degenerate a_u and b_{3u} levels in D_{2h} symmetry (see Fig. 5a).[4–6] Of particular importance is the distinct separation of the first (empty) and second (filled) highest branches, with the Fermi level falling in the energy gap region (0.128 eV). The electronic band structure corresponds to semiconducting behavior, with a room-temperature conductivity (σ_{RT}) of 0.4 S cm^{-1} and an activation energy (E_a) of 0.11 eV (Fig. S2 in the Supporting Information).

********** Figure 3 **********

(coronene)$_5$(GaCl$_4$)$_2$ (2). Salt **2** also belongs to a triclinic lattice with space group $P\bar{1}$,[18] and the asymmetric unit contains two (**A** and **B**) and a half (**C**) coronene molecules and one $GaCl_4^-$ anion. As shown in Fig. 4a, **A** and **B** molecules form a π-stacking column with an **AABB** repeating unit along the *b*–*a* direction, which is flanked by another coronene molecule (**C**). In the column, the parallel **A**–**A** and **B**–**B** pairs have ring-over-atom and ring-over-bond overlap motifs, respectively, whereas neighboring **A** and **B** molecules are non-parallel with a dihedral angle of about 2.2°. Notably, the interplanar distance within an **A**–**A** pair (3.42 Å) is significantly longer than that within a **B**–**B** pair (3.29 Å). Considering that cationic coronene molecules in a dimer approach each other to stabilize the partially occupied HOMO, as described above,[20] this obvious difference in interplanar distances strongly suggests the formation of a charge-disproportionated state within the π-columns in **2**; namely, charge-poor (charge $\delta \approx 0$) **A** and charge-rich (charge $\delta \approx +1$) **B**. The charge-disproportionated state was further confirmed by in-plane Jahn-Teller (JT) distortion and the first-principle calculations (*vide infra*).

********** Figure 4 **********

Each **A** molecule is connected with two neighboring **C** molecules through C–H···π hydrogen bonds (H3···C51: 2.76 Å, H10···C58: 2.75 Å, H10···C60: 2.70 Å vs. sum of van der Waals radii; 2.9 Å[19,28]) and a $GaCl_4^-$ anion through a C–H···Cl hydrogen bond (H9···Cl2: 2.92 Å). On the other hand, each **B** molecule only has short contacts with a **C** molecule through C–H···π hydrogen bonds (H34···C52: 2.87 Å, H34···C53: 2.86 Å, H34···C60: 2.89 Å).

As shown in Fig. 4b, each **C** molecule located at an inversion center is connected with two neighboring $GaCl_4^-$ anions through a C–H···Cl hydrogen bond (H49···Cl2: 2.87 Å) within the *ab* plane at $z \approx 0$. The two-dimensional sheet composed of [$GaCl_4^-$···**C**···$GaCl_4^-$] triads separates the neighboring π-stacking columns composed of **A** and **B**.

Our previous crystallographic study confirmed the unidirectional distortion of cationic coronene molecules in $(coronene)_3M_6O_{19}$ stemming from a static JT effect.[12] The lowering of molecular symmetry from D_{6h} to D_{2h} ("compressed" or "elongated" in Fig. 5a; also see Table S2), which relates to the removal of orbital degeneracy, is adequate to rationalize the in-plane distortion through comparison with the structures optimized by DFT calculations. Figures 5b–g display the deviation of each rim carbon atom (numbered in Fig. 5b) from the average distance of the atoms from the molecular centroid ($\Delta d_i = d_i - \Sigma d_i/12$, where d_i is the distance of carbon atom with a number i from the molecular centroid). As shown in Fig. 5d, coronene molecules in **1** are apparently distorted in an elongated fashion. This distortion bears a quantitative resemblance to that of the D_{2h}-symmetric coronene monocation with a $^2B_{3u}$ electron configuration instead of the ^2A_u electron configuration (Fig. 5c), which was found for $(coronene)_3M_6O_{19}$.[12] Notably, the $^2B_{3u}$ electron configuration is consistent with the result of the DFT calculations, which predict the a_u-derived bands are more stable than the b_{3u}-derived

bands. The root-mean-square of Δd_i ($d_{RMS} = (\Sigma \Delta d_i^2/12)^{1/2}$) for **1** was estimated to be 0.97 × 10^{-2} Å, which is comparable to that estimated from the theoretically optimized coronene monocation with the $^2B_{3u}$ electron configuration (1.20 × 10^{-2} Å). Taking into account the 1:1 stoichiometry, as well as the crystallographic equivalency, it is apparent that all the coronene molecules in **1** are uniformly monocationic, and therefore, the resulting dimers are in a dicationic state.

********** Figure 5 **********

As shown in Figs. 5e–g, the molecular distortions of **A**–**C** in **2** are quite different from each other; **A** and **C** display no remarkable distortions, whereas **B** is apparently distorted in a compressed fashion, as in the case of $(coronene)_3M_6O_{19}$.[12] Indeed, the d_{RMS} value (0.96 × 10^{-2} Å) of **B** is significantly larger than those of **A** (0.46 × 10^{-2} Å) and **C** (0.22 × 10^{-2} Å), and these results provide compelling evidence for charge disproportionation in **2**. The 5:2 stoichiometry of **2** may lead to nearly neutral states (charge $\delta \approx 0$) for **A** and **C**, and a nearly monocationic state (charge $\delta \approx +1$) for **B**, which is in excellent agreement with the above demonstration of longer interplanar distance within an **A**–**A** pair than that within a **B**–**B** pair.

Another way to assess the charge state of coronene molecules is to measure the Raman spectra in the A_{1g} mode region,[6,12,29] although it would be premature to give a quantitative evaluation at the present stage. As shown in Fig. 6, the Raman spectrum of **1** exhibits a single Lorentzian band identified with the A_{1g} mode centered at 1368.9 cm^{-1}. The shift of this band to higher wavenumbers by 2–3 cm^{-1} compared with those of neutral coronene molecules in (coronene)(TCNQ) (1365.7 cm^{-1}) and pristine solid (1366.4 cm^{-1})[12,29] is attributed to the uniform oxidation of coronene molecules in **1**, as indicated by the above results.

********** Figure 6 **********

The Raman spectrum of **2** also shows no indication of distinct splitting of the A_{1g} band (1367.8 cm^{-1}), although the crystallographic study indicates the coexistence of coronene molecules with different charge states. Thus, it appears that the charge disproportionation in **2** is not significant enough to split the band. To help understand these experimental results, we turn to the cobweb charts showing the JT effect in Fig. 5. It appears that the chart for **A** shows a slight but evident molecular distortion, and the d_{RMS} value (0.46×10^{-2} Å) substantially exceeds that of **C** (0.22×10^{-2} Å), as well as those of coronene molecules in a pristine solid (0.17×10^{-2} Å) and a neutral CT complex (coronene)(TCNQ) (0.27×10^{-2} Å).[13,14,30] Although it is difficult to assess the contribution from the dynamic and pseudo (or second-order) JT effects by means of X-ray diffraction measurements, this may be attributed to significant but partial charge disproportionation within the π-columns, with charged states of $+x$ for **A** and $+(1–x)$ for **B** ($x >> 0$).

Figure 7 shows the band dispersion and density of states (DOS) of **2** calculated by using the first principles method with DFT based on the crystallographic data obtained at 100 K (Table S3). The 10 branches in this figure consist of five non-degenerate HOMO and five non-degenerate HOMO-1, arising from the five coronene molecules in each unit cell. Except for the branches arising from **C**, the dispersions of the branches are comparable within the Γ–X and Γ–Y regions, which is attributed to the π-stacking column composed of **A** and **B** along the b–a direction. The width of the highest and second highest bands was estimated to be 95 and 128 meV, respectively. Notably, the charges calculated using a DFT-based tight-binding model analysis are approximately +0.4 for **A**, +0.6 for **B**, and 0 for **C**, which is consistent with the experimental (single-crystal X-ray diffraction and Raman) data. The band gap opening at the Fermi level (0.051 eV) appears to be responsible for the semiconducting

behavior with σ_{RT} = 2.8 S cm^{-1} and E_a = 0.14 eV (Fig. S2 in the Supporting Information).

********** Figure 7 **********

Conclusion

In this study, electrochemical oxidation gave two kinds of coronene cation salts with unprecedented charge arrangements, *i.e.*, π-columnar structures composed of fully charged and charge-disproportionated coronene molecules. The 1:1 salt, (coronene)($GaCl_4$), involves π-columnar zig-zag chains of coronene monocations, which form dicationic face-to-face dimers. In the 5:2 salt, (coronene)$_5$($GaCl_4$)$_2$, there are two kinds of coronene molecules within the π-stacking column with different degrees of JT distortion and different interplanar distances within each pair. Raman spectra and first principles calculations revealed that the charge disproportionation in the π-columns is apparent, but not complete. The calculated band structure of each salt exhibits a gap opening at the Femi level, resulting in semiconducting behavior. Notably, in the present salts, π-stacking columns, which are indispensable for the realization of π-conduction pathways, involve entirely different charge and electronic states from those in previously reported (coronene)$_3M_6O_{19}$ formed with O_h-symmetric $M_6O_{19}^{2-}$ ions.[12] The present results suggest the possibility of developing a new series of molecular (super)conductors with degenerate frontier orbitals by virtue of selecting unexplored counter ions (shape, size, and charge state). Studies along this line are now in progress.

Experimental Section

General Details. Dichloromethane was used as received from Wako Chemicals, and methanol and ethanol were distilled prior to use. Coronene ($C_{24}H_{12}$; Tokyo Kasei, 98%) was

recrystallized several times from distilled benzene. An electrolyte, $(Et_4N)GaCl_4$, was synthesized by reaction of equivalent amounts of $(Et_4N)Cl$ and $GaCl_3$ in ethanol under a nitrogen atmosphere and recrystallized twice from ethanol.

Syntheses of 1 and 2. Salts **1** and **2** were obtained by galvanostatic electrooxidation of coronene in an H-shaped glass cell. The cell was assembled in a glove box filled with argon gas (H_2O, O_2 < 1 ppm). Typically, coronene (*ca.* 5 mg for **1** and *ca.* 11 mg for **2**) and $(Et_4N)GaCl_4$ (*ca.* 30 mg for **1** and *ca.* 50 mg for **2**) were added to the anodic and cathodic compartments, respectively, which are separated by a glass frit. After the cell was vacuum dried, 18 mL of dichloromethane and a few drops of methanol were added to the cell. A constant current (2 μA) was passed between the two platinum electrodes at 15 °C. Black rod crystals grew on the anodic electrode over about two weeks. The obtained crystals were washed with a minimum amount of dichloromethane and methanol, and then dried in air for a few hours.

X-Ray Structural Analysis. Single-crystal X-ray diffraction experiments were performed on a CCD-type diffractometer (Bruker SMART APEX II) with graphite-monochromated Mo Kα radiation (λ = 0.71073 Å) at 100 K. A single crystal was mounted on a glass capillary and cooled by a stream of cooled nitrogen gas. The crystal structures were solved by a direct method using the SIR2004 program[31] and were refined by a full-matrix least-squares method on F^2 using the SHELXL program.[32] All non-hydrogen atoms were anisotropically refined. The positional parameters of the hydrogen atoms were calculated under the assumption of a fixed C–H bond length of 0.93 Å with an sp^2 configuration of the parent atoms. In the refinement procedures, isotropic temperature factors with magnitudes 1.2-fold greater than those of the equivalent temperature factors of the parent atoms were applied to the hydrogen atoms.

Resistivity Measurements. Electrical resistivity was measured using a conventional

four-probe method. Gold wires (ϕ = 15 μm) were attached to a single crystal with carbon paint. A DC current of less than 10 μA was applied along the stacking direction (crystal long axis). After the measurements, we performed the X-ray diffraction measurements on the crystals to identify the crystal lattice.

Raman Measurements. Raman scattering spectra were measured at room temperature in a backscattering geometry, using a microscopic Raman system (Renishaw inVia). The wavelength of the excitation laser is 488 nm. The polarization configuration is (*xx*), where the *x* direction is parallel to the crystal short axis and normal to the stacking direction.

Theoretical Calculations (Single Molecule). DFT calculations with the B3LYP functional[33] were carried out with the 6-31+G(d,p) basis set.[34,35] To ensure the reliability of the frequencies, both "Opt=Tight" and "Int=Ultrafine" were specified. The stabilities of the wave functions were confirmed by specifying the "Stable=Opt" keyword in the present DFT calculations. All the computations were performed using the Gaussian 09 program package,[36] in which the coronene molecule lies on the *yz* plane.

Theoretical Calculations (Band). Electronic structures were obtained using DFT with a generalized gradient approximation[37] as implemented in the quantum-ESPRESSO code.[38] Ultrasoft pseudo-potentials[39] and the plane-wave basis set with cutoff energies of 30 Ry for wavefunctions and 150 Ry for charge densities were used. A tight-binding model based on the maximally-localized Wannier orbitals was constructed using the wannier90 code.[40,41] The charge disproportionation was calculated using this tight-binding model.

Acknowledgements. This work was supported by the Japan Society for the Promotion of Science (JSPS) KAKENHI Grant Numbers JP25288041 and JP16H04139 (YY), JP16H00924 (TK), JP15K17901 (YN), JP26288035 (HY), JP26110512 and JP16H00964 (HK), and JP23225005 (GS) and by JST PRESTO (TK). Theoretical calculations were partly

performed at Research Center for Computational Science, Okazaki, Japan, and the SuperComputer System, Institute for Chemical Research, Kyoto University, Japan.

Supporting Information Available: Photographs of single crystals (Fig. S1), temperature dependence of resistivity (Fig. S2), calculated intermolecular transfer integrals for **1** (Table S1), calculated energies of JT-distorted coronene monocations (Table S2), calculated intermolecular transfer integrals for **2** (Table S3), and X-ray crystallographic data in CIF format. This material is available free of charge via the Internet at http://pubs.acs.org.

Corresponding Author

Phone: +81-52-838-2552. Fax: +81-52-833-7200. E-mail: yyoshida@meijo-u.ac.jp.

References

(1) *Organic Electronics: Materials, Manufacturing, and Applications*; Klauk, H., Ed.; Wiley-VCH, Weinheim, 2006.

(2) Kim, F. S.; Ren, G.; Jenekhe, S. A. *Chem. Mater*. **2011**, *23*, 682–732.

(3) Wang, C.; Dong, H.; Hu, W.; Liu, Y.; Zhu, D. *Chem. Rev*. **2012**, *112*, 2208–2267.

(4) Hoijtink, G. J. *Mol. Phys.* **1959**, *2*, 85–95.

(5) Kato, T.; Yamabe, T. *Chem. Phys. Lett.* **2005**, *403*, 113–118.

(6) Yoshida, Y.; Isomura, K.; Kumagai, Y.; Maesato, M.; Kishida, H.; Mizuno, M.; Saito, G. *J. Phys.: Condens. Matter* **2016**, *28*, 304001.

(7) Pysh, E. S.; Yang, N. C. *J. Am. Chem. Soc.* **1963**, *85*, 2124–2130.

(8) Mortensen. J.; Heinze, J. *Angew. Chem.* **1984**, *23*, 84–85.

(9) Glowatzki, H.; Gavrila, G. N.; Seifert, S.; Johnson, R. L.; Räder, J.; Müllen, K.; Zahn, D. R. T.; Rabe, J. P.; Koch, N. *J. Phys. Chem. C* **2008**, *112*, 1570–1574.

(10) Kasemann, D.; Wagner, C.; Forker, R.; Dienel, T.; Müllen, K.; Fritz, T. *Langmuir* **2009**, *25*, 12569–12573.

(11) Hughes, J. M.; Hernandez, Y.; Aherne, D.; Doessel, L.; Müllen, K.; Moreton, B.; White, T. W.; Partridge, C.; Costantini, G.; Shmeliov, A.; Shannon, M.; Nicolosi, V.; Coleman, J. N. *J. Am. Chem. Soc.* **2012**, *134*, 12168–12179.

(12) Yoshida, Y.; Isomura, K.; Kishida, H.; Kumagai, Y.; Mizuno, M.; Sakata, M.; Koretsune, T.; Nakano, Y.; Yamochi, H.; Maesato, M.; Saito, G. *Chem. Eur. J.* **2016**, *22*, 6023–6030.

(13) Yoshida, Y.; Shimizu, Y.; Yajima, T.; Maruta, G.; Takeda, S.; Nakano, Y.; Hiramatsu, T.; Kageyama, H.; Yamochi, H.; Saito, G. *Chem. Eur. J.* **2013**, *19*, 12313–12324.

(14) Yoshida, Y.; Kumagai, Y.; Mizuno, M.; Saito, G. *Cryst. Growth Des.* **2015**, *15*, 1389–1394.

(15) Yoshida, Y.; Kumagai, Y.; Mizuno, M.; Isomura, K.; Nakamura, Y.; Kishida, H.; Saito, G. *Cryst. Growth Des.* **2015**, *15*, 5513–5518.

(16) Geiser, U.; Schlueter, J. A. *Chem. Rev.* **2004**, *104*, 5203–5241.

(17) Saito, G.; Yoshida, Y. *Bull. Chem. Soc. Jpn.* **2007**, *80*, 1–137.

(18) Crystal data for **1**: $C_{24}H_{12}Cl_4Ga_1$, M = 511.89, triclinic space group $P\bar{1}$, a = 6.8399(6) Å, b = 12.6082(12) Å, c = 13.0793(12) Å, α = 118.191(1)°, β = 75.989(1)°, γ = 98.640(1)°, V = 963.72(15) Å^3, Z = 2, T = 100 K, d_{calc} = 1.764 g cm^{-3}, μ(Mo Kα) = 1.991 mm^{-1}, F(000) = 510, 3919 independent reflections, 262 refined parameters, R_1 = 0.0405 [for $I > 2\sigma(I)$], wR_2 = 0.1037 (for all data), GOF = 1.032; CCDC 1485701. Crystal data for **2**: $C_{120}H_{60}Cl_8Ga_2$, M = 1924.86, triclinic space group $P\bar{1}$, a = 13.2661(10) Å, b = 13.4501(11) Å, c = 14.5575(11) Å, α = 63.678(1)°, β = 69.807(1)°, γ = 62.966(1)°, V = 2040.0(3) Å^3, Z = 1, T = 100 K, d_{calc} = 1.567 g cm^{-3}, μ(Mo Kα) = 0.982 mm^{-1}, F(000) = 978, 8104 independent reflections, 586 refined parameters, R_1 = 0.0383 [for $I > 2\sigma(I)$], wR_2 = 0.0985 (for all data), GOF = 1.021; CCDC 1485702.

(19) Bondi, A. *J. Phys. Chem.* **1964**, *68*, 441–451.

(20) Rapacioli, M.; Spiegelman, F. *Eur. Phys. J. D* **2009**, *52*, 55–58.

(21) Bacon, G. E. *Acta Crystallogr.* **1951**, *4*, 558–561.

(22) Robertson, J. M.; White, J. G. *J. Chem. Soc.* **1945**, 607–617.

(23) Ruuska, H.; Pakkanen, T. A. *J. Phys. Chem. B* **2001**, *105*, 9541–9547.

(24) Grimme, S. *J. Comput. Chem.* **2004**, *25*, 1463–1473.

(25) Grimme, S.; Mück-Lichtenfeld, C.; Antony, J. *J. Phys. Chem. C* **2007**, *111*, 11199–11207.

(26) Podeszwa, R. *J. Chem. Phys.* **2010**, *132*, 044704/1–8.

(27) Sanyal, S.; Manna, A. K.; Pati, S. K. *J. Phys. Chem. C* **2013**, *117*, 825–836.

(28) Nishio, M. *CrystEngComm* **2004**, *6*, 130–158.

(29) Yoshida, Y.; Maesato, M.; Kumagai, Y.; Mizuno, M.; Isomura, K.; Kishida, H.; Izumi, M.; Kubozono, Y.; Otsuka, A.; Yamochi, H.; Saito, G.; Kirakci, K.; Cordier, S.; Perrin, C. *Eur. J. Inorg. Chem.* **2014**, *2014*, 3871–3878.

(30) Chi, X.; Besnard, C.; Thorsmlle, V. K.; Butko, V. Y.; Taylor, A. J.; Siegrist, T.; Ramirez, A. P. *Chem. Mater.* **2004**, *16*, 5751–5755.

(31) Burla, M. C.; Caliandro, R.; Camalli, M.; Carrozzini, B.; Cascarano, G. L.; De Caro, L.; Giacovazzo, C.; Polidori, G.; Spagna, R. *J. Appl. Crystallogr.* **2005**, *38*, 381–388.

(32) Sheldrick, G. M. *SHELXL-2013*; University of Göttingen, Germany, 2013.

(33) Raghavachari, K. *Theor. Chem. Acc.* **2000**, *103*, 361–363 and references therein.

(34) Hehre, W. J.; Ditchfield, R.; Pople, J. A. *J. Chem. Phys.* **1972**, *56*, 2257–2261.

(35) Clark, T.; Chandrasekhar, J.; Spitznagel, G. W.; Schleyer, P. V. R. *J. Comp. Chem.* **1983**, *4*, 294–301.

(36) Frisch, M. J.; Trucks, G. W.; Schlegel, H. B.; Scuseria, G. E.; Robb, M. A.; Cheeseman, J. R.; Scalmani, G.; Barone, V.; Mennucci, B.; Petersson, G. A.; Nakatsuji, H.; Caricato, M.;

Li, X.; Hratchian, H. P.; Izmaylov, A. F.; Bloino, J.; Zheng, G.; Sonnenberg, J. L.; Hada, M.; Ehara, M.; Toyota, K.; Fukuda, R.; Hasegawa, J.; Ishida, M.; Nakajima, T.; Honda, Y.; Kitao, O.; Nakai, H.; Vreven, T.; Montgomery, J. A.; Peralta, J. E.; Ogliaro, F.; Bearpark, M.; Heyd, J. J.; Brothers, E.; Kudin, K. N.; Staroverov, V. N.; Kobayashi, R.; Normand, J.; Raghavachari, K.; Rendell, A.; Burant, J. C.; Iyengar, S. S.; Tomasi, J.; Cossi, M.; Rega, N.; Millam, J. M.; Klene, M.; Knox, J. E.; Cross, J. B.; Bakken, V.; Adamo, C.; Jaramillo, J.; Gomperts, R.; Stratmann, R. E.; Yazyev, O.; Austin, A. J.; Cammi, R.; Pomelli, C.; Ochterski, J. W.; Martin, R. L.; Morokuma, K.; Zakrzewski, V. G.; Voth, G. A.; Salvador, P.; Dannenberg, J. J.; Dapprich, S.; Daniels, A. D.; Farkas, O.; Foresman, J. B.; Ortiz, J. V.; Cioslowski, J.; Fox, D. J. Gaussian 09; Gaussian, Inc., Wallingford, CT, 2009.

(37) Perdew, J. P.; Burke, K.; Ernzerhof, M. *Phys. Rev. Lett.* **1996**, *77*, 3865–3868.

(38) Giannozzi, P.; Baroni, S.; Bonini, N.; Calandra, M.; Car, R.; Cavazzoni, C.; Ceresoli, D.; Chiarotti, G. L.; Cococcioni, M.; Dabo, I.; Dal Corso, A.; de Gironcoli, S.; Fabris, S.; Fratesi, G.; Gebauer, R.; Gerstmann, U.; Gougoussis, C.; Kokalj, A.; Lazzeri, M.; Martin-Samos, L.; Marzari, N.; Mauri, F.; Mazzarello, R.; Paolini, S.; Pasquarello, A.; Paulatto, L.; Sbraccia, C.; Scandolo, S.; Sclauzero, G.; Seitsonen, A. P.; Smogunov, A.; Umari, P.; Wentzcovitch, R. M. *J. Phys.: Condens. Matter* **2009**, *21*, 395502.

(39) Vanderbilt, D. *Phys. Rev. B* **1990**, *41*, 7892–7895.

(40) Marzari, N.; Vanderbilt, D. *Phys. Rev. B* **1997**, *56*, 12847–12865.

(41) Mostofi, A. A.; Yates, J. R.; Lee, Y.-S.; Souza, I.; Vanderbilt, D.; Marzari, N. *Comp. Phys. Comm.* **2008**, *178*, 685–699.

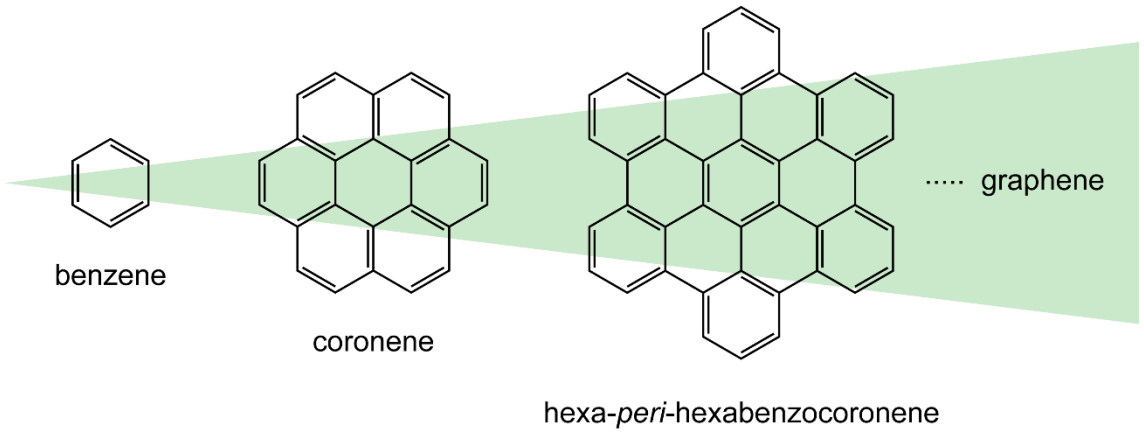

Figure 1. Molecular structures of D_{6h}-symmetric PAH molecules (benzene, coronene, and hexa-*peri*-hexabenzocoronene).

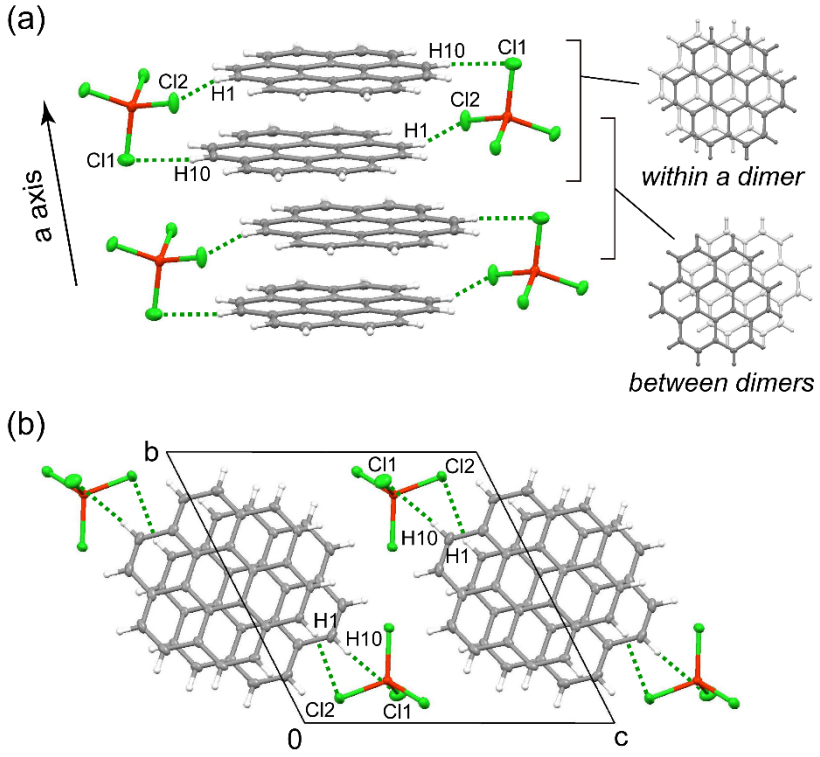

Figure 2. (a) Zig-zag π-columnar structure of coronene cations in (coronene)($GaCl_4$) (**1**), where green dotted lines show C–H···Cl hydrogen bonds between coronene (grey: C, white: H) and $GaCl_4^-$ (red: Ga, green: Cl). Neighboring coronene molecules within the column have a ring-over-atom overlap motif within a dimer and a ring-over-bond overlap motif between dimers. (b) Crystal structure of **1** viewed along the *a* axis.

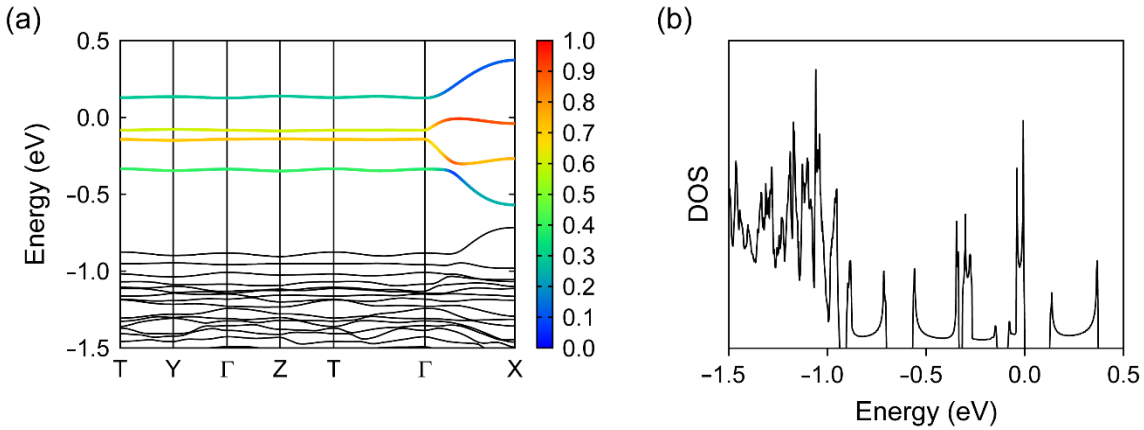

Figure 3. (a) DFT energy band structure and (b) density of states (DOS) of **1**, calculated by first principles methods using the crystallographic data at 100 K, where *T* is (0, 1/2, 1/2) and the energy is given relative to the Fermi energy. In (a), the coloration of the four highest branches represents the fraction of a_u (red) and b_{3u} (blue) components.

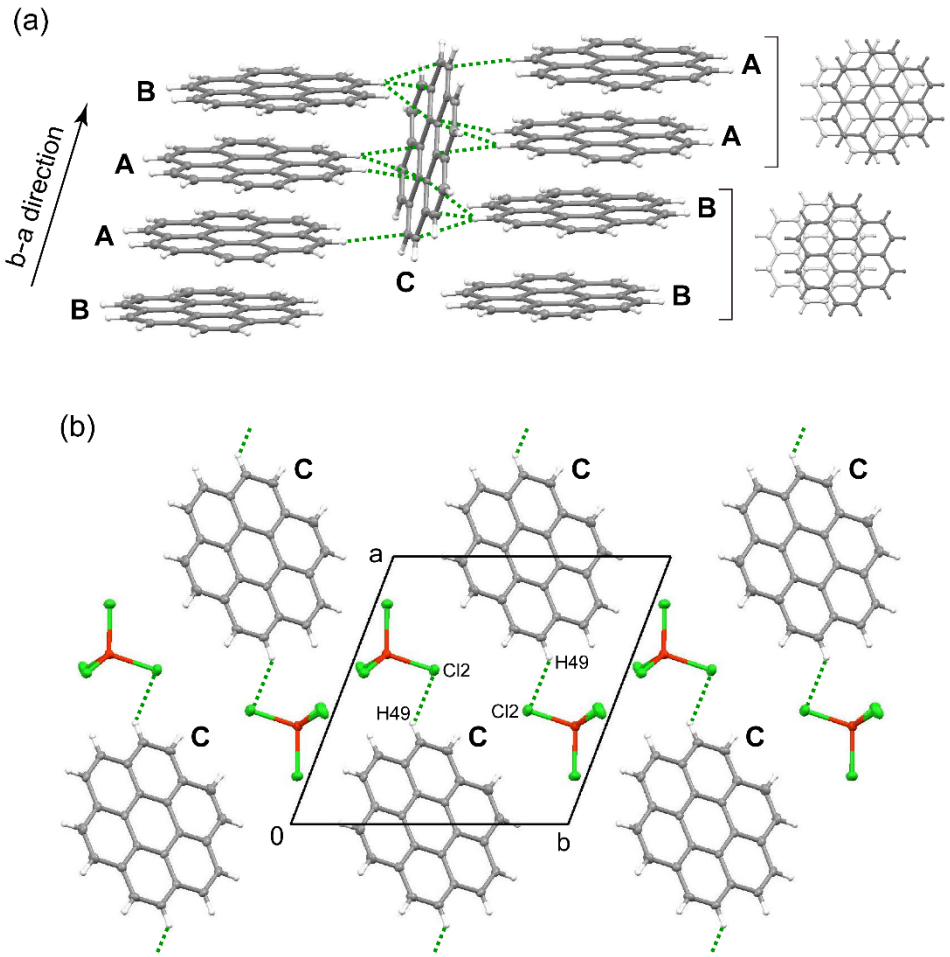

Figure 4. (a) C–H···π hydrogen bonds around **C** in (coronene)$_5$(GaCl$_4$)$_2$ (**2**), where green dotted lines show short C–H···C contacts with H···C distances of less than the sum of the van der Waals radii (2.9 Å). In the π-stacking column with an **AABB** repeating unit along the *b*–*a* direction, the **A–A** and **B–B** pairs have ring-over-atom and ring-over-bond overlap motifs, respectively. (b) Molecular arrangement of **C** and $GaCl_4^-$ within the *ab* plane at $z \approx 0$, where green dotted lines show C–H···Cl hydrogen bonds between **C** and $GaCl_4^-$.

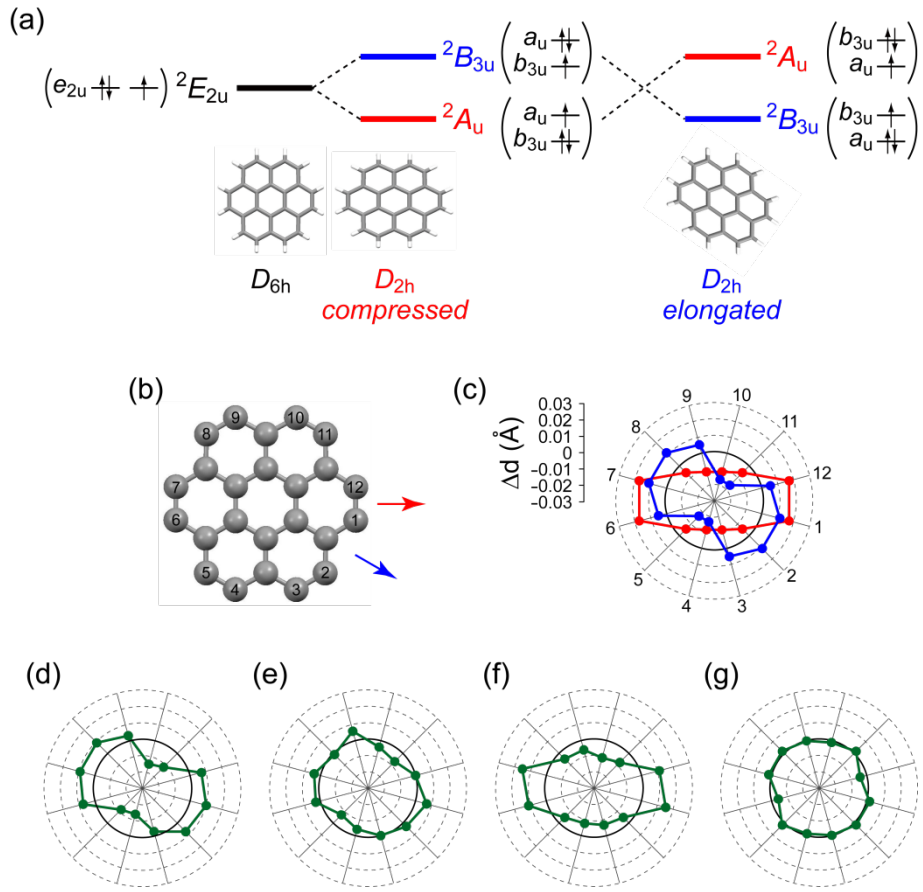

Figure 5. (a) Jahn-Teller (JT) splitting of the ${}^2E_{2u}$ state upon distortion through compression or elongation of the coronene monocation from D_{6h} to D_{2h} symmetry. (b) Molecular structure of coronene, in which the 12 rim carbon atoms are numbered 1–12. Deviations from the average distance of the carbon atoms from the molecular centroid (Δd) are shown on a cobweb chart for (c) D_{2h}-symmetric coronene monocations with structures optimized by DFT calculations (red: compressed distortion with ${}^2A_u$ electron configuration, blue: elongated distortion with ${}^2B_{3u}$ electron configuration),[12] (d) coronene molecule in **1**, and (e) **A**, (f) **B**, and (g) **C** molecules in **2**, where the carbon atom with the highest Δd is numbered 1. All experimental data were obtained at 100 K.

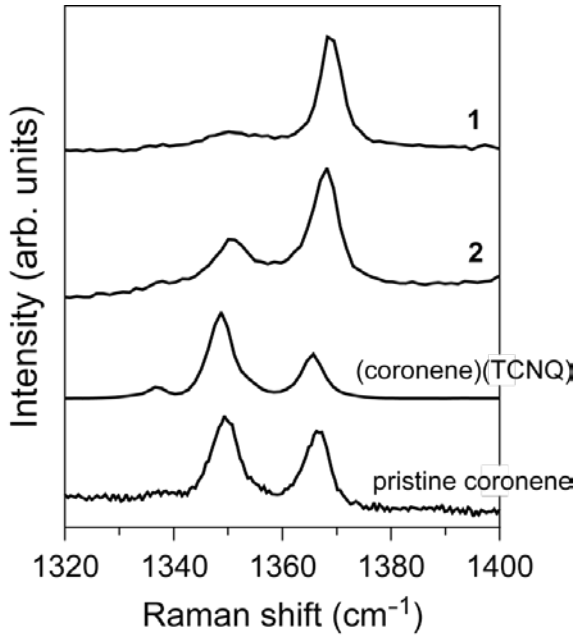

Figure 6. Raman spectra of **1** and **2** at room temperature in the 1320–1400 cm^{-1} region, along with those of a neutral CT complex, (coronene)(TCNQ), and pristine coronene.[12,29]

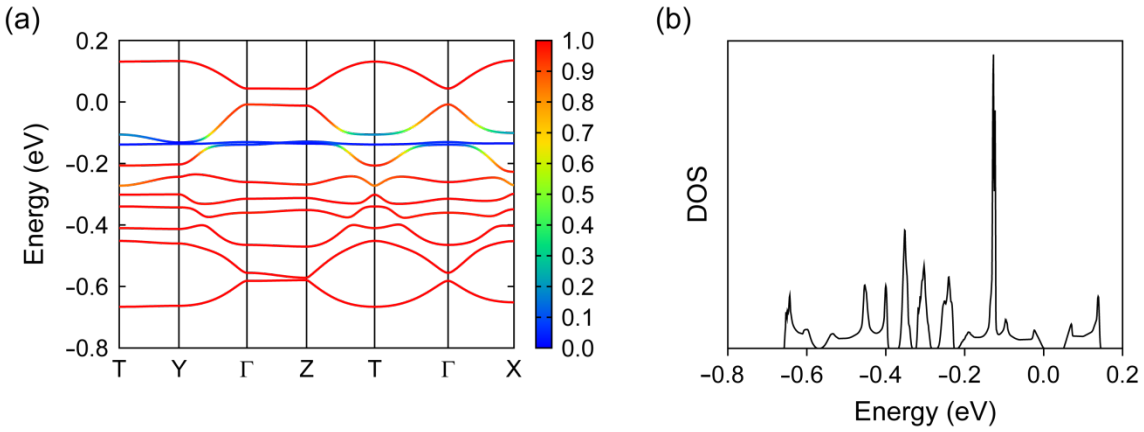

Figure 7. (a) DFT energy band structure and (b) DOS of **2**, calculated by first principles methods using the crystallographic data at 100 K, where *T* is (0, 1/2, 1/2) and the energy is given relative to the Fermi energy. In (a), the coloration of the branches represents the fraction of coronene molecules within the π-columns (**A** and **B**; red) and at the flanking position (**C**; blue).

For Table of Contents Use Only

Title: Cationic π-Stacking Columns of Coronene Molecules with Fully-Charged and Charge-Disproportionated States

Authors: Yukihiro Yoshida, Kazuhide Isomura, Mitsuhiko Maesato, Takashi Koretsune, Yoshiaki Nakano, Hideki Yamochi, Hideo Kishida, and Gunzi Saito

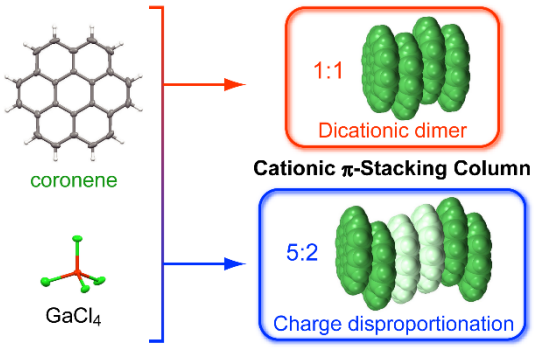

Electrocrystallization gives two kinds of coronene cation salts with different stoichiometries, (coronene)($GaCl_4$) and (coronene)$_5$($GaCl_4$)$_2$. The former salt involves π-stacking columns composed of dicationic coronene dimers. In the latter salt, coronene molecules form a charge-disproportionated π-stacking column flanked by another coronene molecule. The calculated band structure of each salt exhibits a gap opening at the Fermi level, resulting in semiconducting behavior.

Supporting Information

Cationic π-Stacking Columns of Coronene Molecules with Fully Charged and Charge-Disproportionated States

Yukihiro Yoshida,[*,†] Kazuhide Isomura,[‡] Mitsuhiko Maesato,[§] Takashi Koretsune,[#,¶] Yoshiaki Nakano,[§,⊥] Hideki Yamochi,[§,⊥] Hideo Kishida,[‡] and Gunzi Saito[†,‖]

[†] Faculty of Agriculture, Meijo University, Tempaku-ku, Nagoya 468-8502, Japan

[‡] Department of Applied Physics, Nagoya University, Chikusa-ku, Nagoya 464-8603, Japan

[§] Division of Chemistry, Graduate School of Science, Kyoto University, Sakyo-ku, Kyoto 606-8502, Japan

[#] Center for Emergent Matter Science, RIKEN, Wako 351-0198, Japan

[¶] JST, PRESTO, Saitama 332-0012, Japan

[⊥] Research Center for Low Temperature and Materials Sciences, Kyoto University, Sakyo-ku, Kyoto 606-8501, Japan

[‖] Toyota Physical and Chemical Research Institute, Nagakute 480-1192, Japan

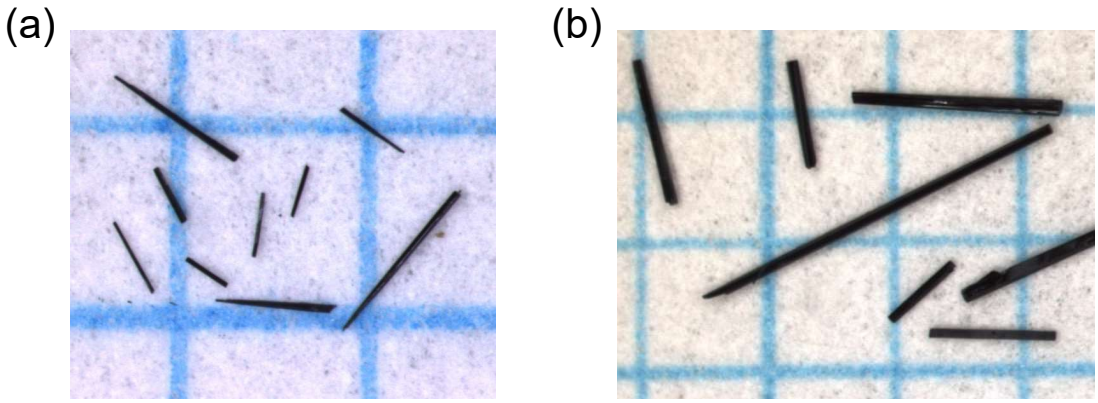

Figure S1. Photograph of rod-shaped crystals of (a) (coronene)($GaCl_4$) (**1**) and (b) (coronene)$_5$($GaCl_4$)$_2$ (**2**) on a millimeter paper.

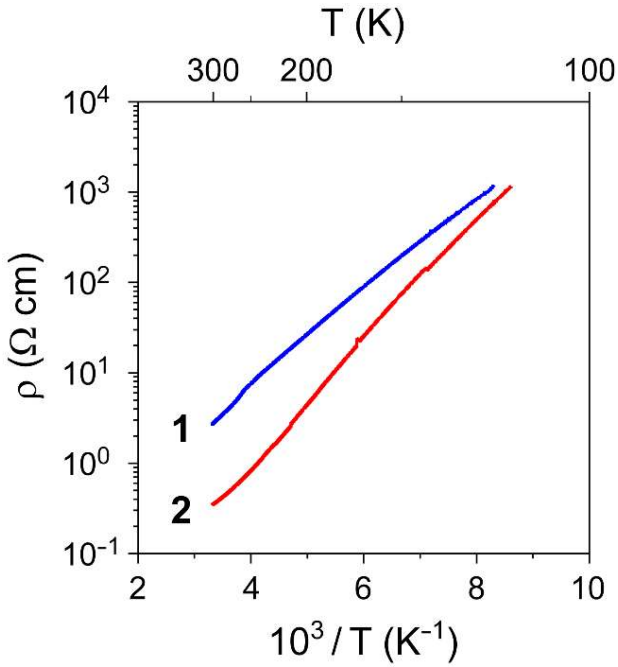

Figure S2. Logarithmic plot of the resistivity (ρ) as a function of reciprocal temperature of a single crystal of **1** (blue) and **2** (red).

Table S1. Intermolecular transfer integrals (> 20 meV) within the column for **1** calculated by first principles methods using the crystallographic data at 100 K

Within a dimer	Transfer integral (meV)
$a_u - a_u$	–120
$b_{3u} - b_{3u}$	–276

Between dimers	Transfer integral (meV)
$a_u - a_u$	59
$b_{3u} - b_{3u}$	135
$a_u - b_{3u}$	–131

Table S2. Point group, state, number of imaginary frequencies (NImag), total and relative energies (E and ΔE), and expectation value of total spin angular momentum ($\langle S^2 \rangle$) of coronene$^+$ at the UB3LYP/6-31+G(d,p) level of theory

Point group	State	NImag	E (hartree)	ΔE (meV)	$\langle S^2 \rangle$
D_{2h}	$^2B_{3u}$	2	−921.68354	0.81	0.769
D_{2h}	^2A_u	1	−921.68355	0.46	0.768
C_{2h}	^2A_u	1	−921.68355	0.46	0.768
C_i	^2A_u	0	−921.68357	0	0.768

Table S3. Intermolecular transfer integrals (> 20 meV) within the column for **2** calculated by first principles methods using the crystallographic data at 100 K[a]

Between A–A	Transfer integral (meV)
a_u-like – a_u-like	166

Between B–B	Transfer integral (meV)
a_u – a_u	62
b_{3u} – b_{3u}	–214

Between A–B	Transfer integral (meV)
a_u-like – a_u	–50
a_u-like – b_{3u}	206
b_{3u}-like – a_u	–41
b_{3u}-like – b_{3u}	–47

[a] Transfer integrals between the neighboring columns are at most about 20 meV.